Crystal Structure and Excited Triplet-State Electron Paramagnetic Resonance of the σ-Bonded TCNQ Dimer in Bis(2,9-dimethyl-1,10-phenanthroline)copper(I) Tetracyanoquinodimethanide, $[Cu(DMP)_2]_2[TCNQ]_2$

Stanislaw K. Hoffmann,[1a] Peter J. Corvan,[1b] Phirtu Singh,[1] C. N. Sethulekshmi,[1] Robert M. Metzger,[2] and William E. Hatfield*[1]

Contribution from the Departments of Chemistry, The University of North Carolina at Chapel Hill, Chapel Hill, North Carolina 27514, and The University of Mississippi, University, Mississippi 38677. *Received August 23, 1982*

Abstract: Reaction of bis(2,9-dimethyl-1,10-phenanthroline)copper(I) iodide $[Cu(DMP)_2I]$ with lithium tetracyanoquinodimethanide, LiTCNQ, yields the compound $[Cu(DMP)_2]_2[TCNQ]_2$, which crystallizes in the triclinic system, space group $P\bar{1}$, with lattice parameters $a = 12.784$ Å, $b = 13.400$ Å, $c = 12.136$ Å, $\alpha = 113.51°$, $\beta = 112.58°$, and $\gamma = 62.80°$. The structure of the compound was solved by Fourier methods and refined by least-squares techniques to $R = 0.060$ on the basis of 1957 observed reflections. The structure consists of $[Cu(DMP)_2]^+$ cations and exocyclically σ-bonded $[TCNQ]_2^{2-}$ dimers. The carbon–carbon bond in the dimer is 1.630 (13) Å, and the $[TCNQ]_2^{2-}$ dimeric ions are arranged in linear chains along the $[\bar{1}10]$ direction. Single-crystal electron paramagnetic resonance studies have been carried out in the temperature range 300–490 K, and thermally activated triplet-state ($S = 1$) EPR spectra as well as doublet-state ($S = {}^1/_2$) EPR spectra have been detected and thoroughly characterized. The data show that strongly localized triplet excitons on $[TCNQ]_2^{2-}$ anions (self-trapped Frenkel excitons) give rise to triplet-state EPR spectra with zero-field splitting parameters $|D/hc| = 0.0111$ cm^{-1} and $|E/hc| = 0.0015$ cm^{-1}. Theoretical calculations of the dipolar splitting indicate that the electronic and molecular structure of the excited state of the $[TCNQ]_2^{2-}$ dimeric anion is best characterized by two distorted $TCNQ^-$ anions with a distorted distribution of spin densities. An EPR signal at $g = 2.0025$ has been attributed to isolated $TCNQ^-$ radical anions. The activation energies for the triplet excitons (which corresponds to the breaking of the σ-bond) and for the isolated $TCNQ^-$ radical anions are 0.55 and 0.24 eV, respectively.

Introduction

Crystals of many salts of $TCNQ^-$ exhibit highly anisotropic physical properties.[3-7] TCNQ is a strong electron acceptor and occurs principally as the radical anion $TCNQ^-$ or as weakly π-bonded dimers that often stack to form quasi-linear anionic chains. Often the linear chains are segregated and consist of uniformly or alternatingly spaced stacks of $TCNQ^-$ anions that are sometimes interspersed with neutral TCNQ molecules. Frequently, highly anisotropic electrical conductivities are observed with the highest electrical conductivity coinciding with the chain-propagation direction. The diffusion or hopping of electrons along the chain gives rise to a motional averaging of EPR lines, and usually very narrow lines are observed ($\Delta B_{pp} \simeq 0.1$ G, where 1.0 G = 0.1 mT). These may exhibit anomalous angular dependences of line widths near the chain or stack axes.[8,9]

There also exist weakly conductive crystals (conductivity below 10^{-9} Ω^{-1} cm^{-1}) of TCNQ salts in which transport mechanisms are not effective.[10] Usually the TCNQ moieties are not stacked in these latter, weakly conductive crystals, although dimer formation may still occur. In addition to the usual π-bonded dimers there are reports of two compounds that exhibit dimer formation through an unusually long, exocyclic, aliphatic carbon–carbon σ bond.[11,12]

Table I. Crystal Data and Data Collection Summary for $Cu(C_{14}H_{12}N_2)_2(C_{12}H_4N_4)$

form. wt	684.3	cryst dimens, mm	0.38 × 0.25 × 0.10
space group	$P\bar{1}$	radiation	Mo Kα (λ 0.710 69 Å)
cell dimens			
a, Å	12.784 (6)	μ, cm^{-1}	7.1
b, Å	13.400 (6)	$2\theta_{max}$, deg	27.5
c, Å	12.136 (4)	scan type	$\omega/2\theta$
α, deg	113.51 (3)	unique data measd	4500
β, deg	112.58 (3)	unique data used	1957
γ, deg	62.80 (3)	$[F_o^2 > 3\sigma(F_o^2)]$	
U, Å^3	1643.0	R	0.060
Z	2	R_w	0.070

These unusual dimers are found in $[Pt(2,2'\text{-bpy})_2][TCNQ]_2$[11] and in $(NEP)_2[TCNQ]_2$ (NEP is *N*-ethylphenazinium).[12] The magnetic properties of these compounds are very interesting. EPR doublets (spectra due to thermally activated triplet states) have been observed in single-crystal samples. Analogous EPR spectra have also been detected in π-bonded dimers,[13-17] trimers,[13,15,18] and tetramers.[15,19-21]

A phase transition to a paramagnetic phase has been observed for $[Pt(bpy)_2][TCNQ]_2$.[11,22] The absence of hyperfine structure

(1) University of North Carolina. (a) Permanent address: Institute of Molecular Physics, Polish Academy of Sciences, 60-179 Poznan, Poland. (b) Present address: Eastman Kodak Co., Rochester, NY.
(2) University of Mississippi.
(3) Nordio, P. L.; Soos, Z. G.; McConnell, H. M. *Ann. Rev. Phys. Chem.* **1966**, *17*, 237-260.
(4) Hatfield, W. E., Ed. *NATO Conf. Series 6* **1979**, *1*, 1.
(5) Gordy, W. "Theory and Applications of Electron Spin Resonance"; Wiley: New York, 1980.
(6) Yagubskii, E. B.; Khidekel, M. L. *Russ. Chem. Rev. (Engl. Transl.)* **1972**, *41*, 1011-1026.
(7) Soos, Z. G. *Ann. Rev. Phys. Chem.* **1974**, *25*, 121-153.
(8) Hibma, T.; Kommandeur, J. *Phys. Rev. Sect. B* **1975**, *B12*, 2608-2618.
(9) Takagi, S.; Kawabe, K. *Solid State Commun.* **1976**, *18*, 1467-1470.
(10) Kepler, R. G. *J. Chem. Phys.* **1963**, *39*, 3528-3532.
(11) Dong, V.; Endres, H.; Keller, H. J.; Moroni, W.; Nöthe, D. *Acta Crystallogr., Sect. B* **1977**, *B33*, 2428-2431.
(12) Harms, R. H.; Keller, H. J.; Nöthe, D.; Werner, M.; Gundel, D.; Sixl, H.; Soos, Z.; Metzger, R. M. *Mol. Cryst. Liq. Cryst.* **1981**, *65*, 179-196.
(13) Hibma, T.; Dupuis, P.; Kommandeur, J. *Chem. Phys. Lett.* **1972**, *15*, 17-20.
(14) Maréchal, M. A.; McConnell, H. M. *J. Chem. Phys.* **1965**, *43*, 497-498.
(15) Bailey, J. C.; Chesnut, D. B. *J. Chem. Phys.* **1969**, *51*, 5118-5128.
(16) Harms, R. H.; Keller, H. J.; Nöthe, D.; Wehe, D.; Heimer, N.; Metzger, R. M.; Gundel, D.; Sixl, H. *Mol. Cryst. Liq. Cryst.* **1982**, *85*, 249-255.
(17) Metzger, R. M.; Heimer, N. E.; Gundel, D.; Sixl, H.; Harms, R. H.; Keller, H. J.; Nöthe, D.; Wehe, D. *J. Chem. Phys.* **1982**, *77*, 6203-6214.
(18) Chesnut, D. B.; Arthur, P. *J. Chem. Phys.* **1962**, *36*, 2969-2975.
(19) Chesnut, D. B.; Phillips, W. D. *J. Chem. Phys.* **1961**, *35*, 1002-1012.
(20) Thomas, D. D.; Merkl, A. W.; Hildebrandt, A. F.; McConnell, H. M. *J. Chem. Phys.* **1964**, *40*, 2588-2594.
(21) Flandrois, S.; Amiell, J.; Carmona, F.; Delhaes, P. *Solid State Commun.* **1975**, *17*, 287-290.
(22) Endres, H.; Keller, H. J.; Moroni, W.; Nöthe, D. *Z. Naturforsch., B* **1976**, *31B*, 1322-1325.

0002-7863/83/1505-4608$01.50/0

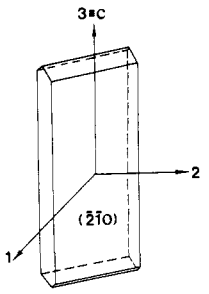

Figure 1. Habit of $[Cu(DMP)_2]_2[TCNQ]_2$ crystal with the orthogonal 1,2,3 coordinate system used in the EPR measurements. Direction cosines of the *a,b,c* crystallographic axes in the 1,2,3 coordinate system are (0.9159, −0.1172, −0.3840), (0.4352, 0.8072, −0.3989), and (0, 0, 1), respectively.

on the thermally activated EPR doublets indicates that the triplet excitons are not localized on TCNQ. This unusual behavior of the EPR in TCNQ crystals has been described in terms of thermally activated Frenkel[17] or Wannier[8] excitons, in terms of the Hubbard Hamiltonian,[23] and by a theoretical band treatment.[24]

Here, we report the synthesis of bis[bis(2,9-dimethyl-1,10-phenanthroline)copper(I)] bis(tetracyanoquinodimethanide) ($[Cu(DMP)_2]_2[TCNQ]_2$), a compound that contains a σ-bonded $[TCNQ]_2^{2-}$ dimer. The compound has been characterized by an X-ray crystal structure determination, and results of studies on thermally activated EPR signals in powdered and single-crystal samples are also analyzed and reported.

Experimental Section

Synthesis. The compound $[Cu(DMP)_2]_2[TCNQ]_2$ was prepared from $Cu(DMP)_2I$[25] and LiTCNQ. To 0.6 g of $Cu(DMP)_2I$ in 100 mL of methanol was added a solution of 0.209 g of LiTCNQ in 50 mL of methanol. The mixture was stirred for 30 min, and the rust-brown precipitate was collected by filtration, washed with 5 mL of cold methanol, and air-dried (yield 0.605 g). Small rust-brown crystals were obtained by recrystallization of the product from 300 mL of hot acetone. As shown in Figure 1, the crystals grow as platelike prisms elongated in the [001] direction with the largest crystal plane being (2̄10). Anal. Calcd for $C_{40}H_{28}N_8Cu$ ($Cu(DMP)_2(TCNQ)$): C, 70.21; H, 4.12; N, 16.38. Found: C, 69.92; H, 4.01; N, 16.20.

X-ray Crystallographic Studies. A crystal of approximate dimensions 0.35 × 0.25 × 0.10 mm was mounted on a eucentric goniometer head and was used for measuring cell dimensions and intensities at 292 K on an Enraf-Nonius CAD-4 computer-controlled diffractometer equipped with a molybdenum X-ray tube and a graphite monochromator. The cell constants were determined by a least-squares refinement of the setting angles of 25 high-angle reflections. The cell constants and other crystallographic data are given in Table I.

The intensities were rather weak; only 1957 reflections with intensities greater than 3σ were observed out of a total of 4500 collected up to $\theta = 27.5°$. These were corrected for background and by a Lorentz and polarization factor but were not corrected for absorption. The linear absorption coefficient for Mo Kα radiation is 7.1 cm^{-1}, which is quite small. All calculations were performed with the CAD-4 SDP set of programs on a PDP 11/34 computer, except for the drawings, which were performed on an IBM/370 computer using ORTEP-II.[26]

Structure Refinement. The copper atom was located from an origin-removed Patterson synthesis and the rest of the non-hydrogen atoms by successive difference Fourier synthesis. The methyl hydrogens could not be located, and the remaining hydrogens were placed in calculated positions. The TCNQ moiety, however, was thought to be making an exceptionally short contact with its centrosymmetric counterpart. Specifically, C(38) (which has two cyano groups attached to it) was only 1.63 Å away from C(38′), the latter being in an adjacent TCNQ moiety. It was concluded that these two atoms may be covalently bound, and a bond angle calculation around C(38) immediately showed that the four atoms attached to C(38) were approximately tetrahedrally disposed. This confirmed the conclusion that a dimerization of TCNQ had occurred through the formation of an exocyclic, aliphatic, carbon–carbon σ-bond.

The refinement of the structure by full-matrix least-squares methods proceeded quite smoothly to a final conventional R index of 0.060 and a weighted R index of 0.070. Refinement in the noncentrosymmetric space group, $P1$, was not attempted since the size of the problem would have been too large not only for the computer programs but also for the amount of intensity data available. However, the thermal parameters were well behaved, the final difference Fourier was quite clean (vide infra), and the inter- and intramolecular distances, except for the C(38)–C(38′) distance, were all normal. Considering the quality of the

Table II. Positional Parameters for $[Cu(DMP)_2]_2[TCNQ]_2$

atom	x	y	z
Cu	0.2024 (1)	0.1657 (1)	0.2266 (1)
N1	0.2912 (6)	−0.0048 (6)	0.1474 (6)
N2	0.2259 (7)	0.1894 (7)	0.0794 (7)
N3	0.0359 (6)	0.2423 (7)	0.2643 (7)
N4	0.2601 (6)	0.2436 (6)	0.4153 (6)
N5	0.2681 (9)	0.5235 (8)	−0.0251 (8)
N6	0.5352 (10)	0.4203 (9)	0.3087 (10)
N7	−0.2131 (7)	0.9363 (7)	0.4288 (7)
N8	0.0851 (8)	0.9474 (7)	0.7411 (8)
C1	0.3236 (9)	−0.0989 (8)	0.1843 (10)
C2	0.3913 (10)	−0.2085 (9)	0.1222 (10)
C3	0.4242 (10)	−0.2230 (9)	0.0162 (10)
C4	0.3898 (8)	−0.1237 (8)	−0.0218 (9)
C5	0.3237 (8)	−0.0181 (9)	0.0450 (9)
C6	0.2884 (8)	0.0835 (8)	0.0110 (8)
C7	0.3184 (8)	0.0764 (8)	−0.0918 (8)
C8	0.2854 (9)	0.1790 (9)	−0.1207 (9)
C9	0.2221 (10)	0.2829 (9)	−0.0505 (9)
C10	0.1896 (9)	0.2903 (8)	0.0540 (10)
C11	0.4207 (10)	−0.1318 (10)	−0.1245 (10)
C12	0.3861 (9)	−0.0355 (10)	−0.1593 (9)
C13	0.2809 (10)	−0.0820 (9)	0.2917 (9)
C14	0.1176 (11)	0.4026 (9)	0.1348 (10)
C15	−0.0713 (8)	0.2463 (8)	0.1953 (9)
C16	−0.1781 (8)	0.3135 (9)	0.2375 (9)
C17	−0.1635 (9)	0.3623 (9)	0.3676 (10)
C18	−0.0512 (8)	0.3583 (8)	0.4451 (9)
C19	0.0507 (8)	0.2977 (8)	0.3954 (8)
C20	0.1656 (8)	0.3016 (8)	0.4673 (8)
C21	0.1801 (8)	0.3552 (8)	0.5929 (8)
C22	0.2947 (10)	0.3575 (9)	0.6575 (9)
C23	0.3882 (10)	0.3045 (10)	0.6058 (10)
C24	0.3707 (8)	0.2439 (9)	0.4763 (9)
C25	−0.0299 (9)	0.4106 (9)	0.5754 (9)
C26	0.0792 (9)	0.4105 (9)	0.6443 (10)
C27	0.4716 (9)	0.1854 (11)	0.4095 (11)
C28	−0.0766 (10)	0.1808 (10)	0.0581 (9)
C29	0.2478 (8)	0.6483 (8)	0.2809 (9)
C30	0.1272 (9)	0.7044 (8)	0.2334 (9)
C31	0.0494 (9)	0.7953 (8)	0.3003 (9)
C32	0.0915 (8)	0.8302 (8)	0.4306 (8)
C33	0.2100 (9)	0.7735 (8)	0.4798 (9)
C34	0.2869 (8)	0.6813 (8)	0.4151 (9)
C35	0.3315 (9)	0.5560 (9)	0.2120 (9)
C36	0.2954 (10)	0.5373 (9)	0.0807 (9)
C37	0.4447 (10)	0.4838 (10)	0.2644 (10)
C38	0.0064 (8)	0.9376 (7)	0.5031 (8)
C39	−0.1160 (8)	0.9370 (8)	0.4606 (8)
C40	0.0508 (8)	0.9401 (8)	0.6398 (8)
H2	0.4150	−0.2778	0.1482
H3	0.4737	−0.3015	−0.0271
H8	0.3080	0.1804	−0.1885
H9	0.1923	0.3585	−0.0724
H11	0.4678	−0.2082	−0.1746
H12	0.4085	−0.0395	−0.2302
H16	−0.2593	0.3230	0.1794
H17	−0.2350	0.3989	0.4038
H22	0.3081	0.4001	0.7469
H23	0.4714	0.3021	0.6578
H25	−0.0987	0.4502	0.6151
H26	0.0911	0.4487	0.7348
H30	0.0929	0.6747	0.1439
H31	−0.0339	0.8357	0.2581
H33	0.2418	0.8006	0.5705
H34	0.3665	0.6367	0.4562

(23) Soos, Z. G.; Klein, D. J. *J. Chem. Phys.* **1971**, *55*, 3284–3290.
(24) Vegter, J. G.; Kommandeur, J. *Mol. Cryst. Liq. Cryst.* **1975**, *30*, 11–49.
(25) Hall, J. R.; Marchant, N. K.; Plowman, R. A. *Aust. J. Chem.* **1963**, *16*, 34–41.
(26) Johnson, C. K. Report No. ORNL-3794, Oak Ridge National Laboratory, Oak Ridge, TN.

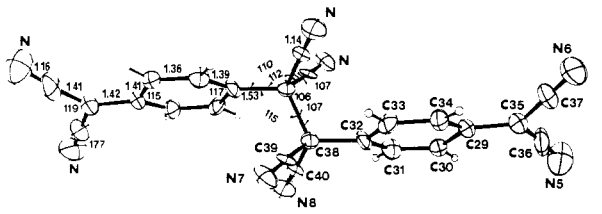

Figure 2. ORTEP view of the TCNQ dimer showing the mean bond distances and angles. There is a crystallographic center of inversion in the middle of the C(38)–C(38′) bond.

data, the space group $P\bar{1}$ was assumed to be correct.

The function minimized was $\sum w[|F_o| - |F_c|]^2$. The weights w were taken to be $4F_o^2/\sigma(F_o)^2$. All atoms except hydrogens were refined with anisotropic thermal parameters; the hydrogens were refined isotropically. All parameter shifts in the last cycle of the refinement were less than 1.0σ. The final difference Fourier showed no peak greater than 0.2 e^-. The final positional parameters are listed in Table II, and the thermal parameters are deposited as supplementary material.

Electron Paramagnetic Resonance Measurements. EPR spectra of powdered and single-crystal samples of $[Cu(DMP)_2]_2[TCNQ]_2$ were recorded with a Varian E-109 spectrometer using a rectangular TE_{102} cavity operating at about 9.17 GHz. The magnetic field was calibrated by means of a Walker-Magnion G-502 NMR gaussmeter and a Hewlett-Packard 5245L frequency counter.

The sensitivity of the spectrometer was calibrated by using a Varian weak-pitch sample and, independently, using a DPPH single crystal (1.275×10^{21} spins/g). Comparison of the results of the calibration measurements indicates that the number of spins in a sample can be estimated with an accuracy of ±50%. Relative changes of the unpaired spins concentrations with temperature can be determined, however, with much higher accuracy (about 0.5%).

The temperature dependences of the EPR spectra were measured in the temperature range 300–490 K by using a Varian E-4557 variable-temperature accessory. The microwave cavity was thermally stabilized by a flux of cooling water. Temperatures were measured with a copper–constantan thermocouple.

Crystals suitable for EPR measurements were very small ($2 \times 0.6 \times 0.1$ mm) platelike prisms. The angular variation measurements were made in the 1,2,3 orthogonal reference system related to the $(\bar{2}\bar{1}0)$ plane as shown in Figure 1. The axis designated 1 is perpendicular to the plane, and the 3 axis coincides with the crystallographic c axis. An optical microscope with a simulated EPR goniometer system was used for accurate alignment of the crystal prior to measurements.

Results

Description of the Structure. The structure is not as accurate as we would have liked, mainly because of the paucity and the weakness of the intensity data. The nominal estimated standard deviations, as obtained from the least-squares matrix, are approximately 0.013 Å in the C–C and C–N bond distances and 1.0° in the bond angles involving C and N atoms.

An ORTEP[26] drawing of the TCNQ dimer is given in Figure 2, which shows that the TCNQ radical anion has indeed dimerized, the dimer bond distance, C(38)–C(38′), being 1.630 (13) Å. This value is comparable to the values 1.631 (4)[11] and 1.65 (2) Å[27] reported previously for this distance in σ-bonded TCNQ dimers. Other bonds to C(38) have also lengthened substantially compared to the similar bonds at the terminal ends of the dimeric moiety. The bond angles at C(38), as shown in Figure 2, are essentially tetrahedral. The dihedral angle between the six-atom ring of TCNQ and the five-atom $C(CN)_2$ plane at the dimerization end is 48°, whereas that at the terminal end is only 13°.

A drawing of the $[Cu^I(DMP)_2]^+$ cation with the atom numbering system is shown in Figure 3. The mean bond distances and angles in the DMP moiety, with assumption of a C_{2v} molecular symmetry, are shown in Figure 4. The distances involving the copper atom are shown on Figure 3. The geometry around the copper atom is essentially tetrahedral, as expected for four-coordinate copper(I) complexes. The distortion from tetrahedral geometry results from the N···N chelate bite of the phenanthroline ligand, which restricts two of the N–Cu–N angles at 82.3 and

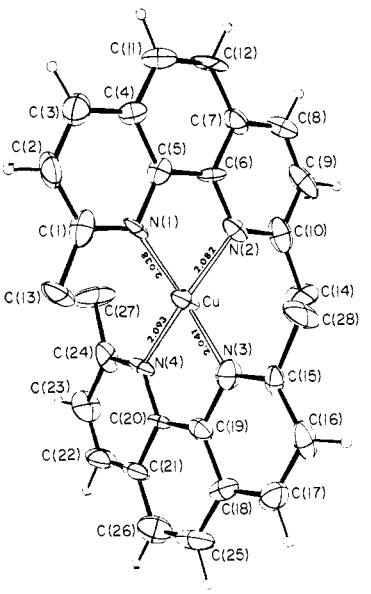

Figure 3. View of the $[Cu(DMP)_2]^+$ cation with the atom numbering system.

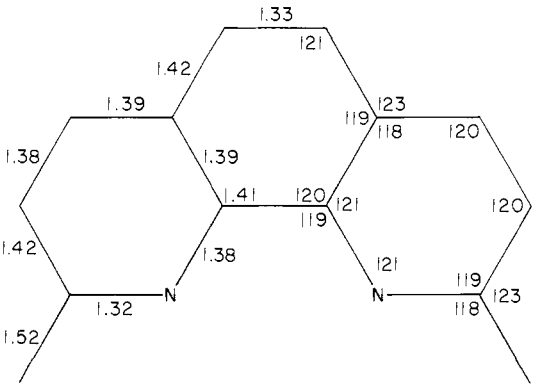

Figure 4. Mean bond distances and angles in the DMP moiety assuming C_{2v} symmetry.

83.4°. The other four N–Cu–N angles range from 120.3 to 129.1°. Each DMP moiety forms a short and a long bond to the copper atom, the short bonds being 2.038 and 2.041 Å and the long bonds being 2.082 and 2.093 Å. The two DMP moieties in the $[Cu(DMP)_2]^+$ cation are approximately perpendicular to each other, the dihedral angle being 97.1°.

There is no interaction between the $[Cu(DMP)_2]^+$ cation and the $[TCNQ]_2^{2-}$ anion except via normal van der Waals separations. One DMP moiety makes an angle of 26.4° and the other an angle of 60.4° with the $[TCNQ]_2^{2-}$ dimer. The latter has its dimer bond close to the b axis with its center located at $(0,0,^1/_2)$ as shown in the stereodiagram in Figure 5. The copper atom and one of the DMP moieties and their centrosymmetrically related counterparts occupy the region around the origin of the cell.

The $[TCNQ]_2^{2-}$ dimers are arranged in chains in the crystal. The chain axis is determined by the symmetry centers $(0,0,^1/_2)$ of the dimers and is parallel to the $[\bar{1}10]$ direction. The neighboring TCNQ molecules in the chain are equidistant with a distance of 8.28 Å between centers of the six-membered rings. Bonding the TCNQ molecules into dimers results in an intradimer distance of 1.63 Å between C(38) and C(38′) and an interdimer distance of 3.88 Å between C(35) and C(35′) at the terminal ends of the adjacent dimers in the chain. The chains are well separated by $[Cu(DMP)_2]^+$ complexes. The chain structure is shown in Figure 6.

Electron Paramagnetic Resonance Results. The EPR spectrum at room temperature consists of one very weak line at the free-radical field position ($g \simeq 2$) with an orientation-dependent line width. With increasing temperature a doublet of EPR lines appears, and this doublet gains intensity with increasing tem-

(27) Morosin, B.; Plastas, H. J.; Coleman, L. B.; Steward, J. M. *Acta Crystallog., Sect. B* **1978**, *B34*, 540–543.

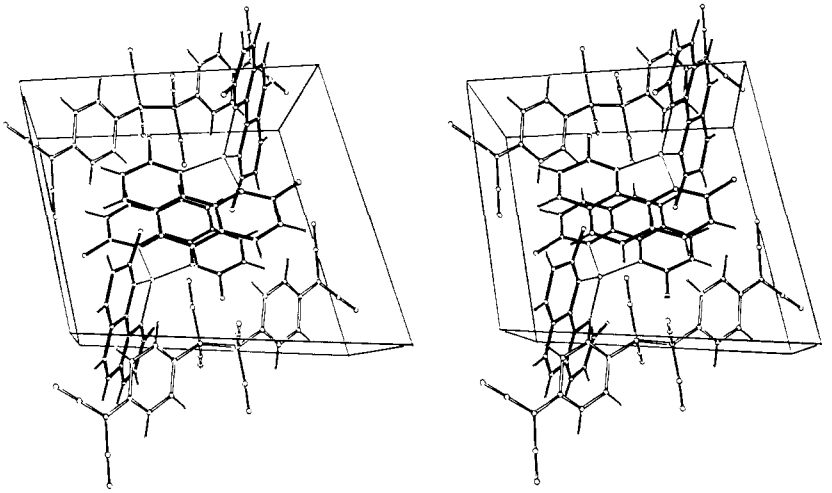

Figure 5. Stereoview of the contents of the unit cell looking down the *a* axis, with the origin in the center, the *b* axis going to the right, and the *c* axis up.

perature. Typical spectra along three orthogonal directions are shown in Figure 7. The doublet spectrum can be identified with the fine structure of an $S = 1$ excited state of the $[TCNQ]_2^{2-}$ dimer. The intensity changes with temperature are fully reversible up to 470 K. At higher temperatures an irreversible decrease in intensity of the triplet fine structure lines is observed as a result of thermal decomposition of the crystal.

A typical high-temperature EPR spectrum consists of a central line at $g = 2.0025$ and two fine structure lines that are comparable in amplitude with the central line and symmetrically displaced from the central line. At some crystal orientations in the magnetic field, when the line width is relatively large, an additional narrow ($\Delta B_{pp} = 1.8$ G) line superimposed on the central line may be observed. Finally, as shown in Figure 8, a half-field transition line ($\Delta M_S = \pm 2$) may be observed at $g \simeq 4$ in the spectra of powdered samples.

We will show that the triplet-state fine structure lines arise from dipole–dipole coupled radical anions that result from the thermal breaking of the long, exocyclic carbon–carbon σ-bond, and that the central line is probably related to isolated $TCNQ^-$ radical anions in the chains described above. No spectral features that could be related to copper(II) complexes or to charge-transfer excited states of the DMP ligand[28] were observed.

Angular Dependence of EPR Spectra. The fine-structure splitting and the line width of the central and fine-structure lines are orientation dependent. These angular variations have been recorded at 10° intervals in the three orthogonal planes of the 1,2,3 coordinate system, and the results are presented in Figure 9.

Triplet-State EPR Spectra. Experimental values of the fine-structure splitting have been fitted to a general second-rank **D** tensor anisotropy equation:[29]

$$\mathbf{D}_i(\theta) = \alpha_i + \beta_i \cos 2\theta + \gamma_i \sin 2\theta \qquad (1)$$

where θ is the azimuthal angle of the magnetic field for the ith rotation of the crystal. The anisotropy parameters α–γ have been calculated for each rotation by least-squares methods. For a constant θ interval, we have the following expressions for the anisotropy parameters:

$$\alpha = n^{-1} \sum_{\theta=0}^{M} D(\theta)$$

$$\beta = 2n^{-1} \sum_{\theta=0}^{M} D(\theta) \cos 2\theta \qquad (2)$$

$$\gamma = 2n^{-1} \sum_{\theta=0}^{M} D(\theta) \sin 2\theta$$

where n and M are determined by the θ interval chosen. These parameters are 36 and 175° for 5° rotation intervals and 18 and 170° for 10° intervals. The anisotropy parameters for the three orthogonal rotations have been corrected for zero-angle errors by a modified Waller–Rogers method[30] using programs written for a Tektronix 4052 microcomputer. The results indicated that the experimental error in angle measurements is less than ±2°. The **D** tensor components were calculated, and the **D** tensor was then diagonalized by standard methods. Principal values and direction cosines are summarized in Table III, and $\mathbf{D}(\theta)$ plots for these data are given by the solid lines in Figure 9. Using the spin Hamiltonian for the $S = 1$ case

$$\mathcal{H} = g\mu_B(B_x\hat{S}_x + B_y\hat{S}_y + B_z\hat{S}_z) + D(\hat{S}_z^2 - \tfrac{2}{3}) + E(\hat{S}_x^2 - \hat{S}_y^2) \qquad (3)$$

we obtained the fine structure parameters $D/hc = -3D_z/2 = \pm 0.0111$ cm^{-1} and $E/hc = (D_y - D_x)/2 = \mp 0.0015$ cm^{-1}. The g factor is isotropic within experimental error, and $g = 2.0025$ (5).

Half-Field Transition. The $\Delta M_s = \pm 2$ forbidden transition is observed in the spectrum of a powdered sample as a single, symmetrical, Lorentzian-shape line with $\Delta B_{pp} = 3.7$ G at 1620.2 G ($g = 4.0430$). Because of the very small size of the crystal used for this study, the half-field line could not be observed in the single-crystal spectrum. The position of the half-field line in a powder spectrum is given by the Kottis–Lefebvre equation:[31]

$$B_{1/2} = (2g\mu_B B_0)^{-1}[(g\mu_B B_0)^2 - 4(D^2 + 3E^2)/3]^{1/2} \qquad (4)$$

Substitution of the measured D and E values (Table III) into eq 4 results in a prediction of $B_{1/2} = 1621.9$ G at $\nu = 9.17$ GHz, which is in good agreement with the experimental value. The intensity ratio of the allowed and forbidden transitions can be evaluated[32] as $(D/g\mu_B B_0)^2 \simeq 1{:}100$. The experimentally estimated value of the intensity ratio was 1:650.

Line Width of Central and Fine-Structure Lines. The central line and the fine-structure lines of the triplet state are of Gaussian shape and the peak-to-peak line width varies with crystal orientation in the range 3–9.8 and 5–12.4 G, respectively. The amplitude (A) of the lines has been measured and relative ΔB_{pp} values have been calculated from the integrated intensity relationship $A(\Delta B_{pp})^2 =$ constant. Angular variations of the ΔB_{pp} presented in Figure 9 indicate the same angular behavior for the triplet-state lines and the central line. This behavior is very similar to that of the **D** tensor. Therefore, the line width of the triplet-state fine-structure lines can also be described as a tensor in the crystal.

(28) Ahn, B. T.; McMillan, D. R. *Inorg. Chem.* **1981**, *20*, 1427–1432.
(29) Weil, J. A.; Buch, T.; Clapp, J. E. *Adv. Magn. Reson.* **1973**, *6*, 183–257.
(30) Waller, W. G.; Rogers, M. T. *J. Magn Reson.* **1975**, *18*, 39–56.
(31) Kottis, P.; Lefebvre, R. *J. Chem. Phys.* **1963**, *39*, 393–403.
(32) Smith, T. D.; Pilbrow, J. R. *Coord. Chem. Rev.* **1974**, *13*, 173–278.

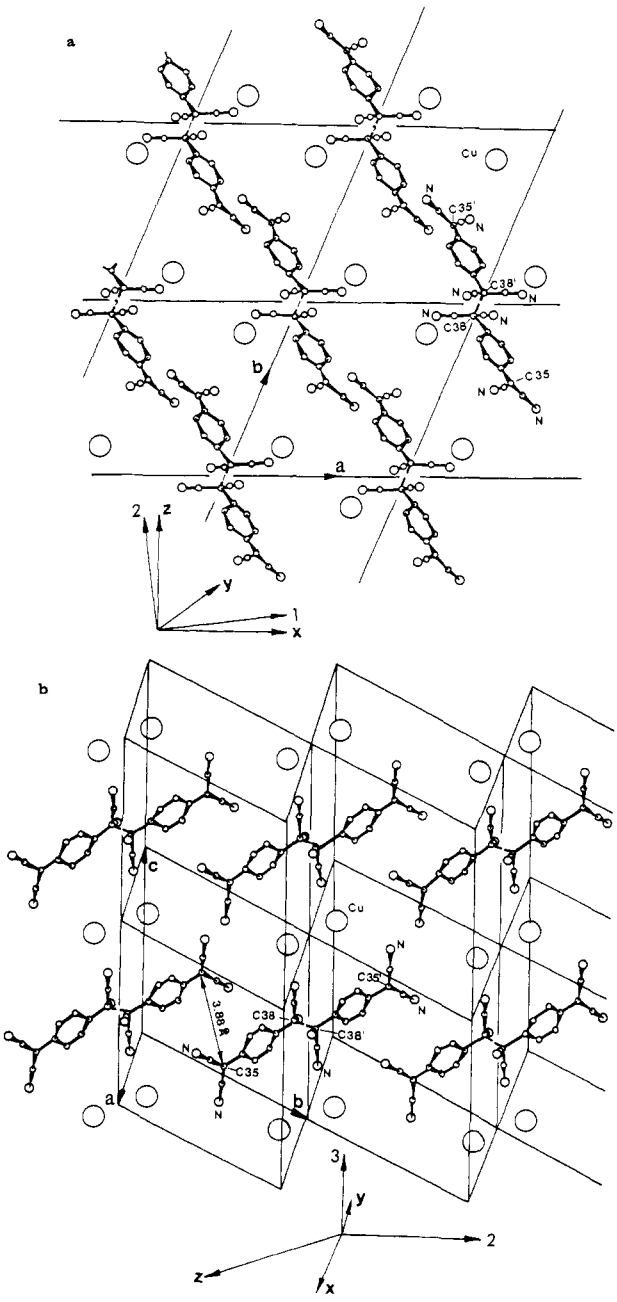

Figure 6. Projection of the $[Cu(DMP)_2]_2[TCNQ]_2$ crystal structure along (a) the c axis (axis 3 of the EPR coordinate system) and (b) the 1 axis of the EPR coordinate system. The unit cell edges and directions of the EPR **D** tensor principal axes x,y,z are indicated. The cation $[Cu(DMP)_2]^+$ is marked only by the position of the Cu(I) ion.

Following the same procedure as in the **D** tensor calculation, the principal values and direction cosines of the ΔB_{pp} tensor were determined and are listed in Table III. Plots of $\Delta B_{pp}(\theta)$ with the parameters given in Table III are given by the solid lines in Figure 9.

Temperature Dependence of the EPR Spectra. Both the central line and the fine-structure lines of the triplet state are thermally activated. At room temperature an impurity signal ($g = 2.0023$) dominates the central line ($g = 2.0025$) in the spectrum. This signal displays Curie law behavior down to 100 K. At higher temperatures the central line increases in intensity and the excited triplet-state fine-structure lines appear. The triplet-state fine-structure lines gain in intensity more rapidly than the central line, and at 395 K the intensities of both types of lines are equal. At higher temperatures the triplet-state fine-structure lines dominate the EPR spectra.

The line widths of the triplet-state fine-structure lines and of the central line are temperature independent. Thus, ΔB_{pp} is not

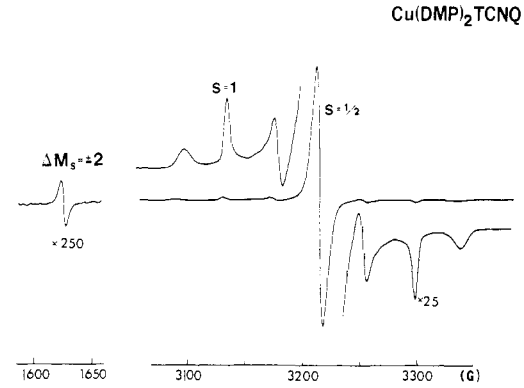

Figure 7. EPR spectrum of a powdered sample of $[Cu(DMP)_2]_2[TCNQ]_2$ at 393 K ($\nu = 9.17$ GHz).

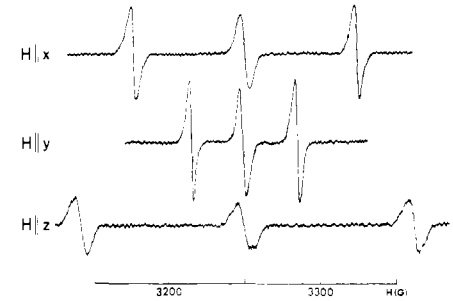

Figure 8. EPR spectrum of a single crystal of $[Cu(DMP)_2]_2[TCNQ]_2$ along the principal directions of the **D** tensor at 328 K. The separations between the outer lines are $|D - 3E| = 3D_{xx}$ for $H||x$, $|D + 3E| = 3D_{yy}$ for $H||y$, and $2|D| = 3D_{zz}$ for $H||z$.

determined by relaxation processes in the crystal. The integrated intensity $I \propto A(\Delta B_{pp})^2$, which is proportional to the number of unpaired spins, is therefore simply proportional to the amplitude of the EPR lines. As shown in Figure 10, the temperature dependence of the EPR spectral intensity is isotropic in single-crystal samples. The g values of the central and fine-structure lines are temperature independent. The fine-structure splitting parameters are also constant over the temperature range studied, except in the region where thermal decomposition occurs. There the splitting decreases slightly with simultaneous broadening of the lines.

Discussion

EPR of the σ-Bonded Dimer $[TCNQ]_2^{2-}$. σ-Bonded TCNQ dimers are rare compared to π-bonded dimers or charge-transfer complexes. The σ-bond may be expected to be relatively weak because of the long bond distance, the considerable delocalization of the bonding electrons, and electrostatic repulsions, Breaking this long, weak σ-bond results in the formation of two $TCNQ^-$ radical anions constrained in close proximity in the solid state. Dipole–dipole and possibly exchange interactions couple these two radical anions into singlet and triplet states. These expectations are borne out by the observation of thermally activated triplet-state EPR spectra in $[Pt(bpy)_2][TCNQ]_2$,[11] $(NEP)_2[TCNQ]_2$,[12] and now $[Cu(DMP)_2]_2[TCNQ]_2$.

The observed excited-state EPR spectrum of the $[TCNQ]_2^{2-}$ dimer has parameters that may be understood in terms of a pairwise dipolar coupling of the unpaired electrons, although an exchange interaction cannot be ruled out completely. The values of the dipolar splitting (**D** tensor components) reflect a spatial distribution of the correlated spins over the TCNQ molecules. The orientation of the **D** tensor principal axes is determined by the symmetry of that distribution, and a knowledge of the unpaired electron density on the constituent atoms of the dimeric pair permits a calculation, in the point–dipole approximation, of the tensor components.

If after bond cleavage the unpaired spins were fully localized on carbon atoms C(38) and C(38′) in the excited state, the **D** tensor should be axially symmetrical and the maximum principal value of the dipolar splitting may be calculated to be 2100 G along

Table III. Electron Paramagnetic Resonance Parameters[a]

	triplet-state spectrum, ($S = 1$)	central line ($S = 1/2$)
	$g = 2.0025$	$g = 2.0025$
	Fine-Structure Tensor	
	$D_x/g_0\mu_B = 56$ G $D_y/g_0\mu_B = 23$ G $D_z/g_0\mu_B = 79$ G $D/hc = \pm 0.0111$ cm^{-1} $E/hc = \pm 0.0015$ cm^{-1}	
	Peak-to-Peak Line Width, G	
$\Delta B_{pp}{}^x$	4.0	6.1
$\Delta B_{pp}{}^y$	3.0	5.0
$\Delta B_{pp}{}^z$	9.8	12.4

Direction Cosines

	D tensor			ΔB_{pp} tensors		
axis[b]	1	2	3	1	2	3
x	−0.8318	0.2896	−0.4736	−0.5435	0.3778	−0.7397
y	−0.5331	−0.1790	0.8269	−0.8245	−0.1406	0.3778
z	0.1547	0.9402	0.3033	0.0960	0.9128	0.3959

[a] Limits of error: g values, ±0.0005; D values, ±1.0 G, ±0.0002 cm^{-1}: ΔB_{pp}, ±0.6 G. [b] See Figure 1.

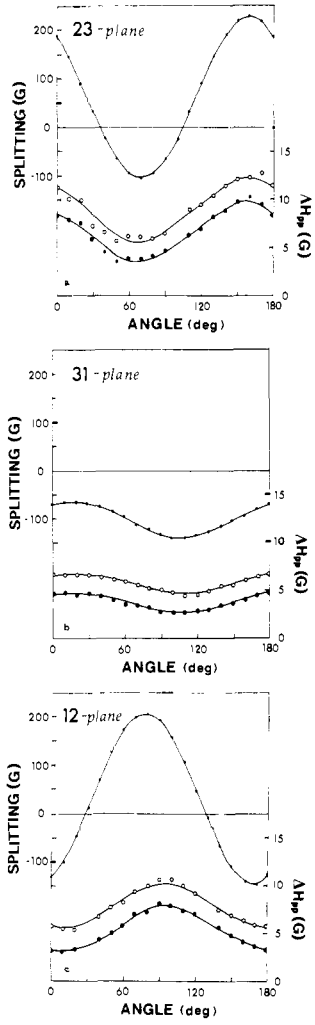

Figure 9. Angular variations of the triplet-state fine-structure and peak-to-peak line widths (filled circles) and central EPR line (open circles) in (a) the 2,3 plane, (b) the 3,1 plane, and (c) the 1,2 plane at 328 K. Solid lines are theoretical plots with the parameters given in Table III.

the C(38)–C(38′) direction. That this approximation strongly overestimates the observed splitting values may be understood in terms of delocalization of the spin density over the $TCNQ^-$ radical anions.

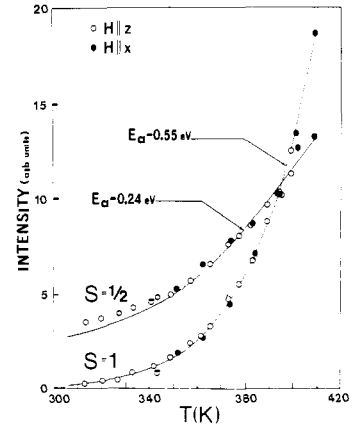

Figure 10. Temperature dependence of the integrated EPR spectral intensity for the triplet-state fine-structure lines ($S = 1$) and the central line ($S = 1/2$) as observed along the z axis (filled circles) and x axis (open circles) of the D tensor. The solid lines are theoretical plots as discussed in the text.

Table IV. Spin Densities in $TCNQ^-$ Anion and $[TCNQ]_2{}^{2-}$ Dianion

	ρ_i	
atom	$TCNQ^-$ normal[12,34]	$[TCNQ]_2{}^{2-}$ distorted[12]
C29	0.109	0.0715
C30	0.059	0.0331
C31	0.059	0.0512
C32	0.109	0.0618
C33	0.059	0.0531
C34	0.059	0.0351
C35	0.191	0.1226
C36	0.002	0.0130
C37	0.002	0.0015
C38	0.191	0.3491
C39	0.002	0.0085
C40	0.002	0.0076
N5	0.039	0.0356
N6	0.039	0.0376
N7	0.039	0.0620
N8	0.039	0.0640

The spin density ρ_i distribution may be calculated by using semiempirical INDO methods and molecular structural data.[33] Such spin density distributions are known for the $TCNQ^-$ anion[34,35]

(33) Pople, J. A.; Beveridge, D. L. "Approximate Molecular Orbital Theory", McGraw-Hill: New York, 1970.

Table V. Experimental and Theoretical Values (for Spin Density Distributions from Table IV) of D Tensor Principal Values and Principal Vector Angles in 1,2,3 Reference System

	$10^{-4}D/hc$, cm^{-1}	direction angles, deg: 1 ∥ $(\bar{2}10)$	2	3 ∥ $[00\bar{1}]$
	Experimental			
D_x	±52	146.3	73.2	118.3
D_y	±22	122.2	100.3	34.2
D_z	∓74	81.1	19.9	72.3
	Theoretical			
two "normal" $TCNQ^-$ ions				
D_x	119.8	148.6	95.6	120.8
D_y	84.8	117.3	109.1	34.3
D_z	−204.6	104.4	20.0	76.5
two "distorted" $TCNQ^-$ ions				
D_x	292.4	148.9	96.3	120.3
D_y	257.1	113.6	118.6	38.5
D_z	−549.5	109.1	29.4	68.5
two "distorted and inverted" $TCNQ^-$ ions				
D_x	56.3	148.3	95.1	121.1
D_y	35.1	118.7	105.3	33.2
D_z	−91.3	102.2	16.2	79.6

and for the excited state of the σ-bonded dimer in $(NEP)_2[TCNQ]_2$.[12] The pertinent data are collected in Table IV. The molecular structure of the σ-bonded $[TCNQ]_2^{2-}$ dimer in $[Cu(DMP)_2]_2[TCNQ]_2$ is similar to that of the dimer in $(NEP)_2[TCNQ]_2$, and we used the ρ_i values from Table IV for calculations of **D** tensor components for a model in which the two $TCNQ^-$ radical anions retain the structure exhibited by the bonded dimer. In the point–dipole approximation those components are given by eq 5. In eq 5, $m,n = x,y,z$ and $r_{ij} = |r_i - r_j|$, and the summation

$$D_{mn} = \tfrac{1}{2}g^2\mu_b^2 \sum_{\substack{i\in A \\ j\in B}} \rho_i\rho_j(r_{ij}^2 - 3m_{ij}n_{ij})r_{ij}^{-5} \qquad (5)$$

runs over all of the atoms in the pairs of $TCNQ^-$ radical anions of a bond-cleaved dimer. D_{mn} values have been calculated from the structural data by using computer programs that have been described previously.[12,17] The results are presented in Table V.

If one uses the spin densities from the ab initio calculation for a $TCNQ^-$ anion with idealized D_{2h} symmetry[34] ("normal" $TCNQ^-$ ion) then the calculated fine-structure tensor components are overestimated by factors of 2.5–4. If, instead, one chooses INDO[33] spin densities calculated[12] for a distorted $TCNQ^-$ $S = {}^1/_2$ ion (with atom positions in the $(NEP)_2[TCNQ]_2$ structure[12]) then the theoretical D_x, D_y, and D_z values ("distorted" $TCNQ^-$ ions in Table V) exceed the experimental values by even larger factors. This arises because the distortion about atom C(38) concentrates the spin density at C(38) (see Table IV), the atom involved (in the ground state) in the exocyclic σ-bond. This increased disagreement between theory and experiment has been noticed before[12] and may be understood in the following way. The expected Coulomb repulsion between the two $TCNQ^-$ radicals in the $S = 1$ state is not relieved by an exchange interaction between the $S = 1$ $[TCNQ]_2^{2-}$ dianion and nearest-neighbor $S = 0$ $[TCNQ]_2^{2-}$ dianions, because of negligible overlap between $[TCNQ]_2^{2-}$ in $[Cu(DMP)_2]_2[TCNQ]_2$ along the $[\bar{1}10]$ chain direction.

Thus, as before,[12] if one uses a triplet-state spin distribution obtained by an inversion of the distorted $TCNQ^-$ radical anion, that is, by interchanging the spin density of C(38) with that of C(35), C(30) with C(37), etc. ("distorted and inverted" $TCNQ^-$ ions in Table V), then much better agreement is obtained between the theoretical and experimental D_x, D_y, and D_z values. This agreement is nearly as good as that obtained between theory and experiment in π-bonded dimers.[14,16,17,35,36]

Table VI. Angles between Crystal Directions and the Principal Axes of the Experimental Tensors and of the Theoretical Fine-Structure Tensor Using the "Distorted and Inverted" Spin Density Distribution

axis	dimer bond C(38)–C(38′)	molecular axis C(38)–C(35)	chain axis $[\bar{1}10]$	cryst axes: *a*	*b*	*c*
		Experimental				
$x(D)$	70.1	105.0	96.4	57.0	66.0	61.7
$y(D)$	67.4	43.1	111.3	34.2	65.3	145.8
$z(D)$	31.9	129.2	22.3	97.9	35.7	107.7
$z(\Delta B_{pp})$	33.7	123.9	22.0	97.1	37.5	113.3
		Theoretical				
$x(D, inv)$	89.3	88.5	117.5	53.7	84.6	58.9
$y(D, inv)$	72.7	37.9	114.7	37.6	70.7	146.8
$z(D, inv)$	17.3	127.9	38.5	81.5	20.1	100.4

Since there is a limited amount of "free space" around the $[TCNQ]_2^{2-}$ dianion in the crystal lattice, one expects some geometrical rearrangement as the dianion is excited from the $S = 0$ to the $S = 1$ state. One may speculate, in particular, that the C(38)–C(38′) distance may increase. As a result it is difficult to predict theoretically the exact equilibrium geometry of the $S = 1$ state. Any fitting of "better" spin densities to experiment in the spirit of ref 36 may be unadvisable since the $TCNQ^-$ ions are, in part, much closer than normal van der Waals distances.

A comparison between the experimental and theoretical orientations of the D_x, D_y, and D_z axes given in Tables V and VI indicates some discrepancies in these values for all three theoretical models. For the "distorted and inverted" spin density model, the largest difference in direction angles between theory and experiment is about 22°. Thus, the symmetry of the spin density distribution is fairly well given by the model and reflects the distortion in the excited state as observed in other crystals.[12,16,17] Experimentally the *z* axis of the **D** tensor deviates 31.9° from the C(38)–C(38′) direction, while the theoretical "distorted and inverted" model predicts a deviation of 17.3°. The data in Table VI also indicate that there is no relationship between the D tensor axes and the TCNQ chain axis $[\bar{1}10]$ in the crystal.

Triplet Excited-State Dynamics. The dynamical behavior of the spins in the triplet state is expected to affect the line width and temperature dependence of the EPR spectrum There are three features of the EPR lines in the spectra of $[Cu(DMP)_2]_2[TCNQ]_2$ that have a bearing on this point: these are the relatively large ΔB_{pp}, the lack of hyperfine splitting of the central and fine-structure lines, and the similarity of the angular variation of ΔB_{pp} with that of the **D** tensor.

The broad EPR lines indicate that the excited state is localized on the $TCNQ^-$ radical anions. Therefore, the data may be described in terms of self-trapping Frenkel excitons. The absence of hyperfine splitting is generally considered to result from a dynamical averaging effect from translation or diffusion of the triplet excitons through the crystal. Theoretical considerations of the line width in TCNQ crystals take into account, moreover, an interchain hopping or diffusion of excitons, and the effect of exciton–exciton interactions.[8,37] Interchain hopping is probably unimportant in determining the line width in $[Cu(DMP)_2]_2[TCNQ]_2$ since the TCNQ chains are well separated by the large $[Cu(DMP)_2]^+$ cations. If exciton–exciton interactions were important, then ΔB_{pp} would be proportional to the density of triplet excitons and show an increase with temperature. As noted above, ΔB_{pp} is independent of temperature in $[Cu(DMP)_2]_2[TCNQ]_2$.

It appears that the line width is due to overlapping and broadening of hyperfine lines. Data for $TCNQ^-$ radical anions[38] indicate that the hyperfine splitting is about 0.52 G for ^{14}N and 0.72 G for ^1H nuclei. Overlapped hyperfine splitting from four

(34) Jonkman, H. T.; van der Welle, G.; Niewport, W. C. *Chem. Phys. Lett.* **1974**, *25*, 62–65.
(35) Silverstein, A. J.; Soos, Z. G. *Chem. Phys. Lett.* **1976**, *39*, 525–530.
(36) Flandrois, S.; Boissonade, J. *Chem. Phys. Lett.* **1978**, *58*, 596–600.
(37) Hibma, T.; Sawatzky, G. A.; Kommandeur, J. *Phys. Rev. Sect. B* **1977**, *B15*, 3959–3966.
(38) Brown, I. M.; Jones, M. T. *J. Chem. Phys.* **1969**, *51*, 4687–4694.

Table VII. Number of Spins and Broken Dimer Bonds at Different Temperatures

	triplet state				central line		
			broken bands				
temp, K	10^{-18}spin/g	10^3spin/mol	ratio	%	10^{-18}spin/g	10^3spin/mol	broken bonds ratio
327	0.12	0.14	1/3570	0.028	1.0	1.2	1/833
394	3.9	4.4	1/114	0.9	3.9	4.4	1/227
409	7.5	8.5	1/59	1.7	5.3	6.0	1/167

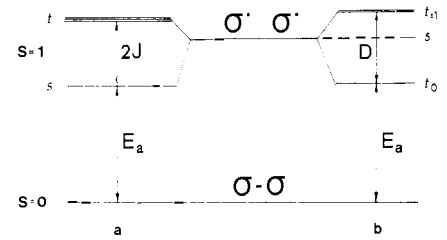

Figure 11. Ground and excited energy levels of the σ-bonded dianion (a) for exchange-coupled dimer (b) for dipole–dipole coupled biradical.

protons and four nitrogen atoms of $[TCNQ]^-$ should result in a broad EPR line ΔB_{pp} of 5–8 G, in good agreement with the ΔB_{pp} values for the triplet-state lines in $[Cu(DMP)_2]_2[TCNQ]_2$ (see Figure 9). Moreover, the lines are Gaussian in shape, as is expected in the case of unresolved hyperfine structure.

The similarity in the angular variation in D and ΔB_{pp} could suggest that the line width may be due to a random distribution of D values in the crystal. This possibility, usual in transition-metal ion EPR spectra, is considered to be a broadening effect arising from randomly distributed strains in crystals.[39,40] This is probably not the case in our crystals since the angular variation of ΔB_{pp} for the triplet lines is identical with that for the central ($S = {}^1/_2$) line, and the central line cannot be related to a distribution of D values. Furthermore, as shown in Table III, the principal directions of the **D** tensor and the $\Delta\mathbf{B}_{pp}$ tensor do not coincide exactly. The broadest EPR line appears along a direction that deviates from the C(38)–C(38′) direction toward the centers of the pairs of dipole-coupled $[TCNQ]^-$ radical anions. This deviation is toward the direction expected for maximum hyperfine splitting from the hydrogen atoms of the six-membered ring, an observation that supports the conclusion that ΔB_{pp} arises from unresolved hyperfine splitting.

Temperature Dependence of Intensities. The integrated intensity I of the triplet-state fine-structure lines is strongly temperature dependent. The value of the intensity is related to the microwave power ($A_0 = \chi_0\omega_0^2B_1^2T_2/4$) absorbed by a sample under resonance conditions. The microwave frequency ω_0 and microwave field intensity B_1 were held constant during intensity measurements. Furthermore, the temperature-independent ΔB_{pp} values indicate that the relaxation time T_2 does not affect the line width. Thus, the EPR line intensity is simply proportional to the static magnetic susceptibility χ_0 of the sample.

The energy levels that are populated and determine the magnetic properties of $[Cu(DMP)_2]_2[TCNQ]_2$ are sketched in Figure 11 for two cases, those being split in the excited state by isotropic exchange only (Figure 11a) or by dipolar interaction only (Figure 11b). It is possible that the excited $S = 1$ state arises from weak antiferromagnetic exchange of the unpaired electrons from the broken σ-bond. In this case the magnetic susceptibility derived from the Van Vleck equation gives the following expression for the relative intensity of the EPR signal:

$$I \propto (1/T)[\exp(-E_a/k_BT)] \times [1 + 3\exp(-E_a/k_BT) + \exp(-E_a/k_BT + 2J/k_BT)]^{-1} \quad (6)$$

A fit of eq 6 to the experimental intensity data yields two results: (i) $E_a = 0.55$ (51.5 kJ/mol) and $2J = 0$; (ii) $E_a = 0$ and $2J = -0.55$ eV. The latter fitting results can be dismissed[56] because the experimental zero-field splitting tensor is traceless within the experimental error in $[Cu(DMP)_2]_2[TCNQ]_2$. Thus, the exchange interaction is very small in the excited state of the $TCNQ_2^{2-}$ dimer and can be estimated to be $J < 10^{-4}$ cm^{-1}. The unpaired electrons are thus essentially coupled by dipolar interaction only, as presented in Figure 11b, with $D/hc = 0.0111$ cm^{-1}. Since the zero-field splitting is much smaller than E_a, this splitting does not influence the magnetic susceptibility of the system. Thus, the system is not a triplet state of the $[TCNQ]_2^{2-}$ dimer but a dipole–dipole coupled biradical with activation energy $E_a = 0.55$ eV. A plot of eq 6 with $E_a = 0.55$ eV and $2J = 0$ is given as the solid line in Figure 10.

The absolute number of spins in the triplet state has been determined as 0.12 (5) $\times 10^{18}$ spins/g at 327 K. The number of broken C(38)–C(38′) σ-bonds producing biradical states as a result of thermal excitations is 0.028% at 327 K and 1.7% at 409 K (see Table VII). If one accepts $E_a = 0.55$ eV as the energy required to break the C(38)–C(38′) σ-bond (with concomitant geometrical rearrangements in the $S = 1$ state), then one should question why the corresponding activation energy is only 0.27 eV in $(NEP)_2[TCNQ]_2$. Either the molecular rearrangement presents a larger Franck–Condon barrier in $[Cu(DMP)_2]_2[TCNQ]_2$, or else the existence of the "chain" of TCNQ dimers in $[Cu(DMP)_2]_2[TCNQ]_2$, albeit with small overlap, provides extra stabilization of the ground state.

Central ($S = {}^1/_2$) EPR Signal. EPR signals at $g \simeq g_e$ are generally observed in TCNQ crystals. In most cases these lines are explained as signals from paramagnetic organic impurities or crystal imperfections. In our crystal, however, at room temperature there are two overlapping lines at $g \simeq g_e$. At room temperature and below there is a broad thermally activated line that nearly obscures a narrow line that gains in intensity as the temperature is decreased. The narrow line with Curie–Weiss behavior is attributed to an impurity or defect signal. The broader, thermally activated line ($g = 2.0025$) exhibits the same angular dependence of line width as the triplet-state fine-structure lines, and we speculate that it arises from isolated $TCNQ^-$ radical anions or $[TCNQ]_2^-$ ions that result from disproportionation according to the following:

$$2[TCNQ]_2^{2-} \rightleftharpoons [TCNQ]_2^- + TCNQ^{2-} + TCNQ^-$$

The behavior of the broader central line is similar to that found in morpholinium TCNQ salts.[7,10] The signal is thermally activated with an EPR line intensity $I \propto (1/T)\exp(-E_a/k_BT)$. The experimental data gives $E_a = 0.24$ eV (22.6 kJ/mol) for temperatures greater than 350 K. Below this temperature the impurity signal is comparable in amplitude with the central line, and the experimental points deviate from the $I(T)$ dependence observed at higher temperatures. The number of spins responsible for the central signal is equal to 3.9×10^{18} spins/g at 394 K, where the intensities of the triplet state fine structure signals and the central signal are identical.

A further very narrow EPR signal ($g = 2.0025$) that is observed only at higher temperatures and is superimposed on the central line can be related to a small number of highly mobile $TCNQ^-$ lattice misfits. These mobile misfits give rise to the motionally narrowed EPR line as a result of a translational motion along the TCNQ chain.

Conclusions

In $[Cu(DMP)_2]_2[TCNQ]_2$, $TCNQ^-$ radical anions are arranged in chains with σ-bonds between pairs of $TCNQ^-$ ions. The σ-bond

(39) Feher, E. R. *Phys. Rev. A* **1964**, *A136*, 145–156.
(40) Hagen, W. R. *J. Magn. Reson.* **1981**, *44*, 447–469.

Table VIII. Zero-Field Splitting Parameters and Activation Energies for σ- and π-Bonded Dimers in TCNQ Compounds[a]

compound	$10^{-4}D/hc$, cm^{-1}	$10^{-4}E/hc$, cm^{-1}	E_a, eV	EPR ref	X-ray str ref
		σ-Bonded Dimers			
1. $[Pt(bpy)_2][TCNQ]_2$	100	14	0.25	11	11
2. $(NEP)_2[TCNQ]_2$	104	14	0.27	12	27
3. $[Cu(DMP)_2]_2[TCNQ]_2$	111	15	0.55	this work	this work
		π-Bonded Dimers			
4. $Li_2[TCNQ]_2$	154	23	0.23	13	
5. $Rb_2[TCNQ]_2$	133	16	0.29	8, 13, 37	41-43
6. $(MPM)_2[TCNQ]_2$	149	18	0.36	14, 15	44
7. $(DMB)_2[TCNQ]_2$	133	23	0.20	13	45
8. $(TMB)_2[TCNQ]_2$	144	22	0.17	8, 13, 37	46
9. $(DMCHA)_2[TCNQ]_2$	141	16	0.31	13	47
10. $(NBP)_2[TCNQ]_2$	124	20	0.14	16	16
11. $(NBP)_2[TCNQF_4]_2$	120	21	0.15	17	55
		π-Bonded Trimeric Dianions			
12. $Rb_2[TCNQ]_3$	94	11		13	
13. $Cs_2[TCNQ]_3$	94	15	0.16	13, 18	48
14. $(MPM)_2[TCNQ]_3$	94	15	0.31	15	49
		π-Bonded Tetrameric Dianions			
15. $(Ph_3PCH_3)_2[TCNQ]_4$	63	10	0.065	15, 19, 20	50, 51
16. $(Ph_3AsCH_3)_2[TCNQ]_4$	63	10	0.065	19	51
17. $(Et_3NH)_2[TCNQ]_4$	41	5	0.036	21	52-54

[a] Abbreviations: bpy, 2,2′-bipyridine; NEP, *N*-ethylphenazinium; DMP, 2,9-dimethyl-1,10-phenanthroline; MPM, morpholinium; DMB, 1,3-dimethylbenzimidazolium; TMB, 1,3,5-trimethylbenzimidazolium; DMCHA, diethylmethylcyclohexylammonium; NBP, *N*-butylphenazinium; $TCNQF_4$, 2,3,5,6-tetrafluorotetracyanoquinodimethane; Ph_3PCH_3, triphenylmethylphosphonium; Et_3NH, triethylammonium.

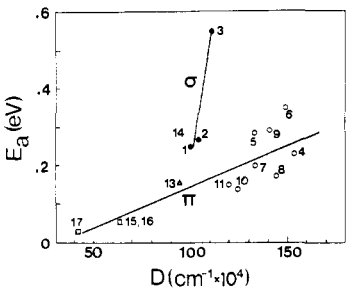

Figure 12. Relationship between the activation energy (E_a) and the fine-structure parameter (D) for σ- and π-bonded TCNQ dimers, trimers, and tetramers. The data points are keyed by number to entries in Table VIII.

is weak and may be thermally cleaved with an activation energy of 0.55 eV. Thermally activated EPR signals are related to a triplet-state arising from dipolar coupling of pairs of $TCNQ^-$ radical anions, and to a doublet state (E_a = 0.24 eV) associated with isolated TCNQ radical anions.

The activation energy for the biradical state arising from bond cleavage is the largest yet observed in sigma bonded $TCNQ^-$ dimers (see Table VIII). The triplet excitations are largely localized, presumably as a result of the structure of the TCNQ chain, which is not optimized for the formation of highly mobile excitons. There was no indication of a phase transition to a paramagnetic phase similar to the phase transition observed in $[Pt(bpy)_2][TCNQ]_2$,[11] even though the structures of $[Cu(DMP)_2]_2[TCNQ]_2$ and $[Pt(bpy)_2][TCNQ]_2$ are similar.

A plot, in Figure 12, of the zero-field splitting parameter D vs. the activation energy for π-bonded TCNQ dimers, trimers, and tetramers and for σ-bonded dimers suggests some correlation between these two quantities for the π-bonded TCNQ molecules. The data used to construct Figure 12 are collected in Table VIII. The D value reflects the spin density values of unpaired electrons on TCNQ molecules in the excited state and also the distance between the molecules. Since the separation between the π-bonded molecules is similar in the different crystals with columnar structures and ranges from 3.15 to 3.60 Å, the difference in D values must arise from differences in ρ values. This is a result of a delocalization of the unpaired electrons over more than one dimer in the columnar structure. In the trimeric and tetrameric clusters of TCNQ molecules we have, formally, two $TCNQ^-$ ions and one or two $TCNQ^0$ neutral molecules, but in effect the charge is distributed over all TCNQ molecules in the cluster, thereby reducing electron–electron repulsions. Thus, the D values are smaller in the trimers than in the dimers and smaller in the tetramers than in the trimers. The strength of the π-bond determines the activation energy and by its distance dependence dominates the D value, therefore leading to the correlation between D and E_a in π-bonded TCNQ compounds. $(Morpholinium)_2(TCNQ)_3$ (compound no. 14) does not adhere to the correlation because of extra stabilization of the ground state of the TCNQ trimer by hydrogen bonding with the morpholinium molecules in the crystal.

The insensitivity of the D values for the σ-bonded dimers to the activation energy implies that the primary interaction leading to the zero-field splitting is not dependent on the population of the triplet state. Thus, D values are intrinsic properties of isolated pairs of coupled radicals arising from the cleavage of the σ-bond. Furthermore, the constancy of the D values indicates that the

(41) Hoekstra, A.; Spoelder, T.; Vos, A. *Acta Crystallogr., Sect. B* **1972**, *B28*, 14-25.
(42) Sakai, N.; Shirotani, I.; Minomura, S. *Bull. Chem. Soc. Jpn.* **1972**, *45*, 3321-3328.
(43) Van Bodegom, B.; de Boer, J. L.; Vos, A. *Acta Crystallogr., Sect. B* **1977**, *B33*, 602-604.
(44) Sundaresan, T.; Wallwork, S. C. *Acta Crystallogr., Sect. B* **1972**, *B28*, 3507-3511.
(45) Chasseau, D.; Gaultier, J.; Hauw, C. *C. R. Acad. Sci., Ser. C* **1972**, *274C*, 1434-1437.
(46) Chasseau, D.; Gaultier, J.; Hauw, C.; Schwoerer, M. *C. R. Acad. Sci., Ser. C* **1972**, *275C*, 1491-1493.
(47) Chonkrown, M. L. Ph.D. Thesis, University of Bordeaux I, 1977.
(48) Fritchie, C. J.; Arthur, P. *Acta Crystallogr.* **1966**, *21*, 139-145.
(49) Sundaresan, T.; Wallwork, S. C. *Acta. Crystallogr., Sect. B* **1972**, *B28*, 491-497.
(50) Konno, M.; Saito, Y. *Acta Crystallogr., Sect. B* **1973**, *B29*, 2815-2824.
(51) McPhail, A. T.; Semeniuk, G. M.; Chesnut, D. B. *J. Chem. Soc. A* **1971**, 2174-2180.
(52) Kobayashi, H.; Ohashi, Y.; Marumo, F.; Saito, Y. *Acta Crystallogr., Sect. B* **1970**, *B26*, 459-467.
(53) Potworowski, J. A. Ph.D. Thesis, University of Toronto, 1973.
(54) Chasseau, D. Thèse, University of Bordeaux I, 1979.
(55) Gundel, D.; Sixl, H.; Metzger, R. M.; Heimer, N. E.; Harms, R. H.; Keller, H. J.; Nöthe, D.; Wehe, D. *J. Chem. Phys.*, in press.
(56) Coffman, R. E.; Buettner, G. R. *J. Phys. Chem.* **1979**, *83*, 2392-2400.

molecular and electronic structure in the triplet state is very similar for all three σ-bonded $[TCNQ]_2^{2-}$ dimers.

Acknowledgment. This research was supported in part by the Office of Naval Research and the National Science Foundation through Grants CHE 80 09685 (University of North Carolina) and DMR 80 15658 (University of Mississippi). We are also grateful to the National Science Foundation for partial funding of the purchase of the EPR spectrometer through Grant CHE 80 06078, and we thank Professor H. J. Keller for insightful discussions.

Registry No. $[Cu(DMP)_2]_2[TCNQ]_2$, 85479-82-9; $Cu(DMP)_2I$, 85479-83-0; LiTCNQ, 1283-90-5.

Supplementary Material Available: Anisotropic thermal parameters (2 pages). Ordering information is given on any current masthead page.

Coordination Chemistry of Microbial Iron Transport Compounds. 22. pH-Dependent Mössbauer Spectroscopy of Ferric Enterobactin and Synthetic Analogues[1]

Vincent L. Pecoraro,[2] Geoffrey B. Wong,[2] Thomas A. Kent,[3] and Kenneth N. Raymond*[2]

Contribution from the Department of Chemistry, University of California, Berkeley, California 94720, and the Gray Freshwater Biological Institute, University of Minnesota, Navarre, Minnesota 55392. *Received April 15, 1982*

Abstract: Iron complexes of the siderophore enterobactin (ent) and the synthetic analogue *N,N',N''*-tris(2,3-dihydroxybenzoyl)-1,3,5-tris(aminomethyl)benzene (MECAM) have been shown through Mössbauer spectroscopy to remain as Fe(III) complexes from pH 2 to 10 in aqueous solution. At high pH and low temperature these two complexes and *N,N',N''*-tris(2,3-dihydroxybenzyl)-1,3,5-tricarbamoylbenzene (TRIMCAM) exhibit both Mössbauer and EPR spectra indicative of high-spin ferric iron in a low-symmetry environment: a broad "4.3" type EPR signal is observed and the 4.2 K Mössbauer spectra are magnetic six-line patterns. At low pH, the magnetic Mössbauer spectrum collapses to a broad quadrupole pair (ΔE_Q = 0.8 mm/s, δ = 0.5 mm/s), indicating that the spin relaxation rate is fast compared with the nuclear precession frequency. At low pH ($\geq$2) titration data show that $[Fe(ent)]^{3-}$ and its close analogue $[Fe(MECAM)]^{3-}$ undergo stepwise protonation in aqueous solution. The ultimate products of this protonation are the insoluble compounds $[Fe(H_3ent)]^0$ and $[Fe(H_3MECAM)]^0$, in which protonation of one catechol oxygen results in a shift to a "salicylate" mode of coordination involving the ortho carbonyl of the 2,3-dihydroxybenzoyl rings. Chemical analysis of the supernatant solutions from these solids show no iron is present. From pH 10 to 2, in solution and the solid state, the complexes remain intact and the iron atom remains as high-spin Fe(III) in a six-coordinate, rhombic environment (g = 4.3). For $[Fe(TRIMCAM)]^{3-}$, a structural isomer of the MECAM complex which does not have a carbonyl group attached to the catechol ring and hence is not capable of the salicylate coordination mode, lowering the pH results in stepwise dissociation of the complex, in contrast to the corresponding enterobactin or MECAM complexes. While $[Fe(ent)]^{3-}$ in neutral aqueous solution cannot readily release its iron by reduction, the potential drops rapidly with pH and reductive release of iron under acid conditions is feasible. In the absence of a specific reductase enzyme, either the internal reduction of ferric ion by enterobactin ligand (to give Fe^{2+} annd semiquinone) in *nonaqueous* solution or the reduction in an acidic, *aqueous* environment of the Fe(III) tris(salicylate) species $Fe(H_3ent)$, which forms below pH 4, provides an alternative to the esterase mechanism of iron acquisition by microbes which use enterobactin in iron uptake. In contrast to the aqueous complex, Fe(ent) *in methanol* at low pH exhibits a quasi-reversible redox chemistry; at a pH meter reading of 1, approximately 45% of the iron is in the ferrous form (ΔE_Q = 3.44 mm/s, δ = 1.38 mm/s).

Iron is an essential element in the chemistry of living systems. Although the metal is relatively abundant in the earth's crust, it is inaccessible to microorganisms under normal conditions due to the formation of insoluble hydroxides. As an evolutionary response to this stress, microbes produce low molecular weight organic ligands (siderophores), which effectively solubilize ferric ion for transport into the cell.[4,5] One such compound is enterochelin[6] (called here enterobactin[7]), synthesized by the enteric bacteria *Salmonella typhimurium*, *Escherichia coli*, and *Klebsiella pneumoniae*. The structure of this cyclic triester of (2,3-dihydroxybenzoyl)serine is diagrammed in Figure 1.

Enterobactin (ent) coordinates ferric ion octahedrally with six oxygens from three catechoyl moieties.[6-12] The resulting molecule possesses the largest formation constant (approximately 10^{52}) of any known ferric complex.[11] It has been proposed that release of iron from $[Fe(ent)]^{3-}$, once inside the cell, proceeds by ligand degradation through enzymatic hydrolysis of the ester linkages.[13] Much of the research into the structure and bonding of enterobactin has been devoted to elucidating the properties of tris(catecholate) coordination in $[Fe(ent)]^{3-}$ at high or neutral pH. Since

(1) Previous paper in this series: Tufano, T. P.; Raymond, K. N. *J. Am. Chem. Soc.* **1981**, *103*, 6617.
(2) Department of Chemistry, University of California, Berkeley, CA. 94720.
(3) Gray Freshwater Biological Institute, University of Minnesota, Navarre, MN 55392.
(4) Neilands, J. B., Ed. "Microbial Iron Metabolism"; Academic Press: New York, 1974.
(5) Raymond, K. N.; Carrano, C. J. *Acc. Chem. Res.* **1979**, *12*, 183.
(6) O'Brien, I. G.; Gibson, F. *Biochim. Biophys. Acta* **1970**, *215*, 393.
(7) Pollack, J. R.; Neilands, J. B. *Biochem. Biophys. Res. Commun.* **1970**, *38*, 989.
(8) Llinas, M.; Wilson, D. M.; Neilands, J. B. *Biochemistry* **1973**, *12*, 3836.
(9) Isied, S. S.; Kuo, G.; Raymond, K. N. *J. Am. Chem. Soc.* **1976**, *98*, 1763.
(10) Spartalian, K.; Oosterhuis, W. T.; Neilands, J. B. *J. Chem. Phys.* **1975**, *63*, 3538.
(11) Harris, W. R.; Carrano, C. J.; Cooper, S. R.; Sofen, S. R.; Avdeef, A.; McArdle, J. V.; Raymond, K. N. *J. Am. Chem. Soc.* **1979**, *101*, 6097.
(12) Cooper, S. R.; McArdle, J. V.; Raymond, K. N. *Proc. Natl. Acad. Sci. U.S.A.* **1978**, *75*, 3551.
(13) (a) O'Brien, I. G.; Cox, G. B.; Gibson, F. *Biochem. Biophys. Acta* **1971**, *237*, 537. (b) Greenwood, K. T.; Luke, R. K. J. *Ibid.* **1978**, *525* 209.

0002-7863/83/1505-4617$01.50/0